June 1994

Deformable Models with Parameter Functions: Application to Heart Wall Modeling

Jinah Park
University of Pennsylvania

Dimitris Metaxas
University of Pennsylvania

Alistair Young
University of Pennsylvania

Copyright 1994 IEEE. Reprinted from *Proceedings of the IEEE Computer Society Conference on Computer Vision and Pattern Recognition*, pages 437-442.
Publisher URL: http://dx.doi.org/10.1109/CVPR.1994.323863

Deformable Models with Parameter Functions: Application to Heart Wall Modeling

Abstract

This paper develops a new class of physics-based deformable models which can deform both globally and locally. Their global parameters are functions allowing the definition of new parameterized primitives and parameterized global deformations. These new global parameter functions improve the accuracy of shape description through the use of a few intuitive parameters such as functional bending and twisting. Using a physics-based approach we convert these geometric models into deformable models that deform due to forces exerted from the datapoints so as to conform to the given dataset. We present an experiment involving the extraction of shape and motion of the Left Ventricle (LV) of a heart from MRI-SPAMM data based on a few global parameter functions.

Deformable Models with Parameter Functions: Application to Heart-Wall Modeling

Jinah Park[1] Dimitri Metaxas[1] and Alistair Young[2]

[1]Department of Computer & Information Science
University of Pennsylvania
Philadelphia PA 19104-6389

[2]Department of Radiology
University of Pennsylvania
Philadelphia PA 19104

Abstract

This paper develops a new class of physics-based deformable models which can deform both globally and locally. Their global parameters are functions allowing the definition of new parameterized primitives and parameterized global deformations. These new global parameter functions improve the accuracy of shape description through the use of a few intuitive parameters such as functional bending and twisting. Using a physics-based approach we convert these geometric models into deformable models that deform due to forces exerted from the datapoints so as to conform to the given dataset. We present an experiment involving the extraction of shape and motion of the Left Ventricle (LV) of a heart from MRI-SPAMM data based on a few global parameter functions.

1 Introduction

Heart disease, a major cause of mortality in the Western World, generally leads to abnormalities of heart wall motion. The major difficulties in assessing heart wall disease among physicians have included 1) the use of imaging techniques (e.g., CT, MRI) where no explicit data correspondence between frames can be provided, 2) the lack of sufficient resolution in the extracted data, and 3) the absence of computational techniques for automatic extraction of the three dimensional heart wall motion parameters in a way that is "useful" to physicians. Recently, a new magnetic resonance imaging (MRI) technique based on magnetic tagging ("SPAMM") was developed at the University of Pennsylvania for imaging of regional heart wall motion [2]. This technique promises to be very useful in the analysis of heart wall motion because it provides temporal correspondence of material points. This correspondence in conjunction with the use of the three dimensional location of each SPAMM tag can subsequently be used as input to a motion analysis technique to extract the three dimensional motion parameters.

Recently, computer vision techniques for reconstructing the 3D shape and motion of the heart's left ventricle (LV) have been developed. Using time varying CT or MRI data, McInerney and Terzopoulos [8] developed a 3D finite element surface model, Huang and Goldgof [5] developed a spring-mass, adaptive-size mesh model, Cohen and Cohen [4] developed a technique to track the 2D slices of the heart's left ventricle using deformable balloons and subsequently reconstruct the ventricle's 3D shape, Pentland and Horowitz [12] developed a technique for approximating the left ventricle's shape using a few modes (linearized, rotation, stretch and bending), and Amini and Duncan [1] developed a technique for motion tracking of the left ventricle wall using bending and stretching thin-plate models. One problem with the above techniques is that they do not capture the twisting motion of the heart, known to occur during systole. Also, they are formulated in terms of either many local parameters that require non-trivial processing to be useful to a physician, or very few parameters that can offer only a gross approximation of the heart's motion. The best technique so far for accurately capturing the shape and motion of a heart's left ventricle is that of Young *et al.* [15] and Moore *et al.* [11] which use 3D finite elements and SPAMM data. Their main limitation is that there is an enormous amount of information on motion and deformation captured. The three-dimensional strain tensor, for example, has three "normal components" and three shear components, each of which may vary with position in the wall. In order to understand the complex relationship between these components and other motion parameters, it is desirable to characterize the motion in terms of a few physical parameters that offer sufficient accuracy.

In this paper we present a new technique that describes the time-varying shape, deformation and shape of the LV in terms of a few "global" *parameter functions*, such as twist, whose value is allowed to vary locally. In this way the complex motion of the heart is described by the same small number of parameters, which vary from region to re-

1063-6919/94 $3.00 © 1994 IEEE

gion. Furthermore, these parameters are intuitive and can be used by a physician without further complex processing. Our approach is based on the development of a new family of parameterized deformable primitives suitable for this application. These deformable primitives are parameterized using global parameter functions whose value varies across the primitive's shape as opposed to being constant [10, 13]. Through the use of appropriate parameterization the axes of our new deformable primitives can be curved. This is a major generalization compared to parameterized primitives such as superquadrics, cylinders and cubes, commonly used in the vision literature. Furthermore, generalized cylinders [3, 7], even though they allow shapes with curved axes, do not offer shape representation in terms of a few parameters. Finally, our new models can represent open[1] parameterized shapes suitable for modeling the shape and motion of the LV.

By incorporating the geometric definition of our new models into our physics-based framework [10] we create models that deform due to forces exerted from the SPAMM data, and conform to the given dataset. The extracted parameters can then be directly used for analysis by a physician after plotting parameter graphs. We applied our technique to various subjects and analyze the results of our parameter extraction. Furthermore, we show visualization results from the model fitting to the various SPAMM data over time and we measure the model's goodness of fit to the data.

2 Geometry of Deformable Models with Parameter Functions

In this section we will introduce a new class of deformable models which allows the use of parameters (global) that can characterize an object's shape in terms of a few parameter functions. Furthermore, even though we will not use them in this paper due to the nature of our experiments, our models can have local deformation parameters [10] to represent shape detail. This functional variation of the global parameters allows the characterization of complex shape with a small number of intuitive parameters. These varying global parameters are independent of the underlying shape to which they are applied. The representation of the underlying shape can be expressed as an arbitrary set of datapoints or a parameterized primitive (e.g., superquadric). Finally, with these new continuous global deformations, we can create models whose x, y, z axes are curved, and can represent open shapes. These new models are a generalization of our previously developed deformable models [10, 13], where the global parameters were constant across the object's shape.

[1] not a closed surface, but more like a cup

In general, our models are 3D solids whose material coordinates $\mathbf{u} = (u, v, w)$ are defined in a domain Ω. The positions of points on the model relative to an inertial frame of reference Φ in space are given by a vector-valued, time varying function $\mathbf{x}(\mathbf{u}, t) = (x_1(\mathbf{u}, t), x_2(\mathbf{u}, t), x_3(\mathbf{u}, t))^\mathsf{T}$, where $^\mathsf{T}$ denotes transposition. We set up a non-inertial, model-centered reference frame ϕ and express the position function as

$$\mathbf{x} = \mathbf{c} + \mathbf{R}\mathbf{p}, \tag{1}$$

where $\mathbf{c}(t)$ is the origin of ϕ at the center of the model and the rotation matrix $\mathbf{R}(t)$ gives the orientation of ϕ relative to Φ. Thus, $\mathbf{p}(\mathbf{u}, t)$ gives the positions of points on the model relative to the model frame. We further express $\mathbf{p} = \mathbf{s} + \mathbf{d}$ as the sum of a reference shape $\mathbf{s}(\mathbf{u}, t)$ and a displacement $\mathbf{d}(\mathbf{u}, t)$.

2.1 Global Deformations

We define the reference shape as

$$\mathbf{s} = \mathbf{T}(\mathbf{e};\, b_0(\mathbf{u}), b_1(\mathbf{u}), \ldots), \tag{2}$$

where $\mathbf{e}$ can represent either a set of 3D points in space[2] or a geometric primitive

$$\mathbf{e}(\mathbf{u};\, a_0(\mathbf{u}), a_1(\mathbf{u}), \ldots) \tag{3}$$

defined parametrically in $\mathbf{u}$ and parameterized by the variables $a_i(\mathbf{u})$. The shape represented by $\mathbf{e}$ is subjected to the *global deformation* $\mathbf{T}$ which depends on the global deformation parameter functions $b_i(\mathbf{u})$.

Although generally nonlinear, $\mathbf{e}$ and $\mathbf{T}$ are assumed to be differentiable[3] so that we may compute the Jacobian of $\mathbf{s}$. $\mathbf{T}$ may be a composite sequence of primitive deformation functions $\mathbf{T}(\mathbf{e}) = \mathbf{T}_1(\mathbf{T}_2(\ldots \mathbf{T}_n(\mathbf{e})))$. We concatenate the global deformation parameters into the vector

$$\mathbf{q}_s = (a_0(\mathbf{u}), a_1(\mathbf{u}), \ldots, b_0(\mathbf{u}), b_1(\mathbf{u}), \ldots)^\mathsf{T}. \tag{4}$$

Equations (2) and (3) define global parameters a_i, b_i that are functions of $\mathbf{u}$, instead of being constants [10]. The above definition allows us to generalize definitions of primitives (e.g., superquadrics, cubes) and parameterized deformations (e.g., twisting, bending) as will be shown in the following examples. For the applications in this paper, we will assume that $a_i(\mathbf{u}) = a_i(u)$ and $b_i(\mathbf{u}) = b_i(u)$, where the material coordinate u corresponds to the longest axis of the deformable model.

2.1.1 Primitives with Parameter Functions

Our technique for creating primitives with parameter functions can be applied to any parametric primitive (e.g., superquadric, cube), by replacing its constant parameters with

[2] In that case the material coordinates $\mathbf{u}$ coincide with the cartesian space in which the 3D points are expressed.

[3] In case where $\mathbf{e}$ is a set of points, the above assumption does not apply.

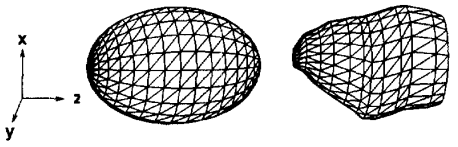

(a) (b)

Figure 1: (a) Superquadric ellipsoid (b) Primitive with parameter functions.

differentiable parameter functions. For our applications, we demonstrate our approach by transforming a superellipsoid primitive to a primitive with parameter functions.

The definition of such a generalized primitive $\mathbf{e} = (e_1, e_2, e_3)^\mathsf{T}$ is given by the following equations

$$\mathbf{e} = a_0(u) \begin{pmatrix} a_1(u) C_u^{\epsilon_1(u)} C_v^{\epsilon_2(u)} \\ a_2(u) C_u^{\epsilon_1(u)} S_v^{\epsilon_2(u)} \\ a_3(u) S_u^{\epsilon_1(u)} \end{pmatrix}, \qquad (5)$$

where $-\pi/2 \leq u \leq \pi/2$, $-\pi \leq v < \pi$, $0 \leq w \leq 1$, $S_\theta{}^\epsilon = \text{sgn}(\sin\theta)|\sin\theta|^\epsilon$ and $C_\theta{}^\epsilon = \text{sgn}(\cos\theta)|\cos\theta|^\epsilon$. Here, $a_0(u) \geq 0$ is a scale parameter function, $0 \leq a_1(u), a_2(u), a_3(u) \leq 1$, are aspect ratio parameter functions, and $\epsilon_1(u), \epsilon_2(u) \geq 0$ are "squareness" parameter functions. We can also define a open parameterized primitive given by the above definition by restricting the ranges of the u and v parameters to a subset of the above definition.

We can generalize the above equation (5) to define a primitive $\mathbf{s}_g$ with curved axis in any directions x, y, and z by the following equation

$$\begin{aligned} \mathbf{s}_g &= \mathbf{T}_o(\mathbf{e}; e_{1_o}(u), e_{2_o}(u), e_{3_o}(u)) \\ &= \begin{pmatrix} e_1 + e_{1_o}(u) \\ e_2 + e_{2_o}(u) \\ e_3 + e_{3_o}(u) \end{pmatrix}, \end{aligned} \qquad (6)$$

where $e_{1_o}(u), e_{2_o}(u)$ and $e_{3_o}(u)$ are axis-offset parameter functions.

Fig. (1)(a) shows a superquadric ellipsoid, while Fig. (1)(b) shows a generalized primitive $\mathbf{s}_g$, where its shape has been obtained by varying the piecewise linear parameter functions $a_3(u)$ and $e_{1_o}(u)$, and the domain of u is a subset of the domain of u (i.e., $-\pi/2 \leq u \leq \pi/4$) for a superellipsoid.

2.1.2 Parameterized Global Deformations with Parameter Functions

Our formulation of global deformations with continuous parameter functions is general and can be applied to any underlying shape $\mathbf{e}$. For our applications in this paper we will define the model which includes bending, twisting and axis offset deformations.

Given a primitive $\mathbf{e}$, we first define the bending of axis 1 along principal axes 2 and 3[4] as a parameterized deformation $\mathbf{T}_b$, which results in the global shape $\mathbf{s}_b = (s_1, s_2, s_3)^\mathsf{T}$:

$$\begin{aligned} \mathbf{s}_b &= \mathbf{T}_b(\mathbf{e}; b_0(u), b_1(u), b_2(u), b_3(u)) \\ &= \begin{pmatrix} e_1 \\ e_2 + b_0(u) cos(\frac{e_1 + b_1(u)}{e_{1_{max}}} \pi) \\ e_3 + b_2(u) cos(\frac{e_1 + b_3(u)}{e_{1_{max}}} \pi) \end{pmatrix}, \end{aligned} \qquad (7)$$

where $b_0(u), b_2(u)$ define the magnitudes of the bending and can be positive or negative, and $-1 \leq b_1(u), b_3(u) \leq 1$ define the locations on axis 1 where the maximum bending occurs. Then we define twisting along principal axis 3, which results in the global shape $\mathbf{s}_{tb}$:

$$\begin{aligned} \mathbf{s}_{tb} &= \mathbf{T}_{twist}(\mathbf{T}_b(\mathbf{e}; b_0(u), b_1(u), b_2(u), b_3(u)); \tau(u))) \\ &= \mathbf{T}_{twist}(\mathbf{s}_b; \tau(u)) \\ &= \begin{pmatrix} s_1 \cos(\tau(u)) - s_2 \sin(\tau(u)) \\ s_1 \sin(\tau(u)) + s_2 \cos(\tau(u)) \\ s_3 \end{pmatrix}, \end{aligned} \qquad (8)$$

where $\tau(u)$ is the twisting parameter function along axis 3. Finally we apply an offset deformation defined in Equation (6) to arrive at the global reference shape $\mathbf{s} = \mathbf{T}_o(\mathbf{s}_{tb}; e_{1_o}(u), e_{2_o}(u), e_{3_o}(u))$. [5]

Note that the choice of the parameter functions depends on the application. For the applications in this paper we assume that those parameter functions are piecewise linear along u, so we do not impose any shape continuity constraints on the LV shape.

2.2 Local Deformations

Local, finite element basis functions are the natural choice for representing the local deformations [13, 9]. The elements have a node at each of their corners. The generalized coordinates of the finite element basis functions are the nodal variables—a vector $\mathbf{q}_{d_i}$ associated with each node i of the model. If we collect the generalized coordinates into a vector of degrees of freedom $\mathbf{q}_d = (\ldots, \mathbf{q}_{d_i}^\mathsf{T}, \ldots)^\mathsf{T}$, we can write $\mathbf{d} = \mathbf{S}\mathbf{q}_d$, where $\mathbf{S}$ is the shape matrix whose entries are the finite element basis functions.

2.3 Kinematics and Dynamics

The velocity of points on the model is given by

$$\dot{\mathbf{x}} = \dot{\mathbf{c}} + \dot{\mathbf{R}}\mathbf{p} + \mathbf{R}\dot{\mathbf{p}} = \dot{\mathbf{c}} + \mathbf{B}\dot{\boldsymbol{\theta}} + \mathbf{R}\dot{\mathbf{s}} + \mathbf{R}\mathbf{S}\dot{\mathbf{q}}_d, \qquad (9)$$

where $\boldsymbol{\theta} = (\ldots, \theta_i, \ldots)^\mathsf{T}$ is the rotational coordinates of the model and $\mathbf{B} = [\ldots \partial(\mathbf{R}\mathbf{p})/\partial\theta_i \ldots]$. Furthermore, $\dot{\mathbf{s}} = [\partial\mathbf{s}/\partial\mathbf{q}_s]\dot{\mathbf{q}}_s = \mathbf{J}\dot{\mathbf{q}}_s$, where $\mathbf{J}$ is the Jacobian of the

[4] The principal axes 1, 2 and 3 correspond to the x, y and z axes of the model frame ϕ.

[5] For the applications in this paper, $a_0(u) = a_0$, $\epsilon_1(u) = \epsilon_2(u) = 1$ and $e_{3_o}(u) = 0$.

generalized primitive with global parameter functions. We can therefore write

$$\dot{\mathbf{x}} = [\mathbf{I}\ \mathbf{B}\ \mathbf{RJ}\ \mathbf{RS}]\dot{\mathbf{q}} = \mathbf{L}\dot{\mathbf{q}}, \tag{10}$$

where $\mathbf{q} = (\mathbf{q}_c^\top, \mathbf{q}_\theta^\top, \mathbf{q}_s^\top, \mathbf{q}_d^\top)^\top$, with $\mathbf{q}_c = \mathbf{c}$ and $\mathbf{q}_\theta = \boldsymbol{\theta}$ expressed as a quaternion [9].

We can make our model dynamic in $\mathbf{q}$ by introducing mass, damping, and a deformation strain energy. The resulting Lagrange equations of motion simplified, for a vision application, by setting the mass density to zero are

$$\mathbf{D}\dot{\mathbf{q}} + \mathbf{K}\mathbf{q} = \mathbf{f}_q, \tag{11}$$

where $\mathbf{D}$ and $\mathbf{K}$ are the damping and stiffness matrices respectively, and where $\mathbf{f}_q(\mathrm{u}, t)$ are the generalized external forces associated with the degrees of freedom of the model. The above equation yields a model that has no inertia and comes to rest as soon as all the applied forces equilibrate or vanish [10].

The generalized forces $\mathbf{f}_q$ are computed using the formula $\mathbf{f}_q = \int \mathbf{L}^\top \mathbf{f}\, d\mathrm{u}$. These forces are associated with the components of $\mathbf{q}$, where $\mathbf{f}(\mathrm{u}, t)$ is the 3D force distribution applied to the model [10].

Since the SPAMM data provides the correspondence over time of individual data points, we apply the force distribution algorithm only once for the initial frame. In subsequent frames the corresponding points will exert a force to the same point on the model as computed in the first frame. In this way we can recover the LV twisting motion.

3 Experiments

Our experiments run at real or interactive time speeds on a Silicon Graphics R4000 Crimson workstation including the real time graphics. Furthermore, through appropriate careful design, large portions of our code have been parallelized making it even faster when multiple processors are available (e.g., on our Silicon Graphics 4D/340VGX shared memory multiprocessor).

We apply our technique to SPAMM data from the LV obtained from the Department of Radiology, University of Pennsylvania (courtesy of Dr. Leon Axel) collected during LV systole over 5 intervals. The SPAMM technique provides data throughout the heart wall. Since our modeling technique is surface based we chose to fit the LV mid-wall motion as this is most accurately defined by the SPAMM imaging technique. In Young *et al.* [14] a technique based on snakes [6] was developed to extract 3D coordinates of SPAMM data from the LV mid-wall.

In this experiment we demonstrate our model fitting technique to time-varying SPAMM data from a normal heart, specifically from the LV mid-wall. Fig. 2(a) shows the model initialized to data from the first frame (end-diastole).

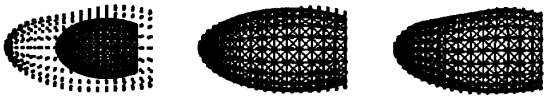

(a) (b) (c)

Figure 2: Fitting a model to a normal heart (LV mid-wall).

Fig. 2(b) shows, for demonstration purposes only, a model with constant parameters (a superellipsoid) fitted to the data. The inadequacy of such a model to obtain an accurate fit is obvious. The average distance error of fitting is 1.3 mm and the RMS error is 0.83 mm (7.5 %), while the length of the LV is approximately 110 mm. Fig. 2(c) shows our deformable model with parameter functions fitted to the data. The improvement is obvious and the average distance error is 0.86 mm and the RMS error is 0.48 mm (4.4 %).

Fig. 3(a) shows the model shown in Fig. 2(c) from a different view point, and Figs. 3(b-e) show the model fitted to subsequent time frames during systole. Figs. 3(f-j) are the surface shaded images of Fig. 3(a-e). We can easily observe the contracting motion as well as the twisting motion of the model. The twisting motion can be observed better in the Figs. 3(a-e), where the veritcal lines of the mesh of the front and the back cross each other progressively due to its twisting motion. The orientation of a model is depicted in Fig. 4.

In Fig. 5 we plot the extracted model parameter functions over the 5 time frames. The graphs in the first column of Fig. 5 show plots of the model's parameter functions $a_1(u), a_2(u)$ and $a_3(u)$, which are associated with its length in the x, y and z directions, respectively. For each frame we plot the ratio of each parameter function during frame $t = 2...5$, with respect to its value at the initial frame ($t = 1$). The first graph in the second column shows plots of the model's twisting parameter function $\tau(u)$. Finally, the remaining two graphs in Fig. 5 show plots of the bending parameter functions $b_0(u)$ and $b_2(u)$ which denote the magnitudes of bending of the x axis in the y and z directions. In all graphs, $U = 0$ corresponds to u_{min} of the model (the apex of the LV), and $U = 16$ corresponds to u_{max} of the model (the base of the LV).

From these graphs, we can quantify the motion and shape changes of the LV during its systole. For example, by studying the graphs of a_1 and a_2, we can conclude that the magnitude of contraction in the radial direction (i.e. along x and y axes) during systole is approximately 20%. But it is not uniform towards the base of the LV where the contraction along y axis (being approximately 10%) is less then one along x axis (being approximately 20%) making the base look more elliptical. This result supports clinical study findings where more stress is exerted at the apex during the LV motion, and also there is an increased closeness

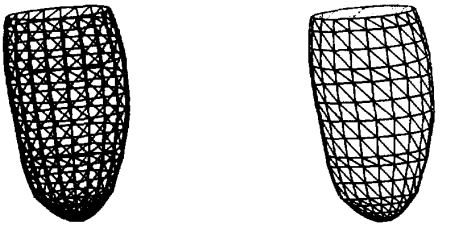

(a) time 1 (f)

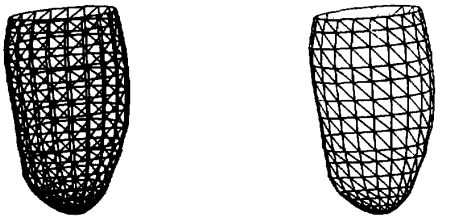

(b) time 2 (g)

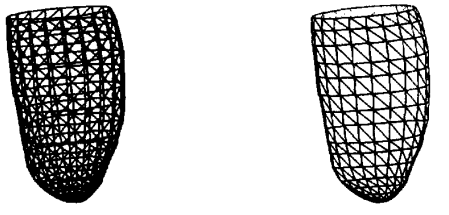

(c) time 3 (h)

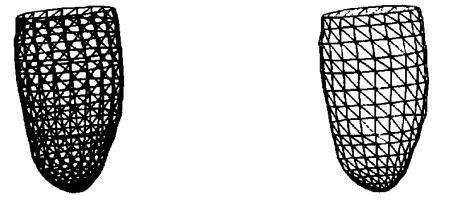

(d) time 4 (i)

(e) time 5 (j)

Figure 3: Model fitted to SPAMM data from a LV mid-wall during systole.

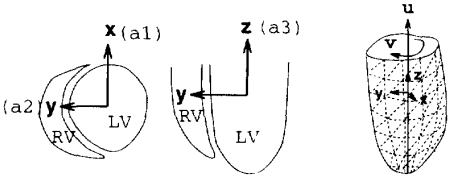

Figure 4: Orientation of the model for Fig.3

to an ellipse of the LV base shape during systole. Contraction along the z axis, known as longitudinal contraction of the LV, during systole is also quantified, from the graph of a_3, to approximately 20%. From the graph of τ (labeled as *twist* in Fig. 5), we can quantify the twisting motion of the LV during systole to approximately 7 degrees. The graph shows a small amount of global rotation before the twisting occurs. Doctors often find this behavior of the LV. Bending parameters in this application capture the v-variations around each ring. The graphs of b_0 and b_1 show the contraction around the apex and at the base of the LV is not just radial.

We have applied our technique to the set of data from another normal heart and have found that the results are similar to those reported in this paper. To compare our results, we have also fitted our model to two sets of data from abnormal hearts with hypertrophic cardiomyopathy. While the results were similar for these two abnormal hearts, they were different from the ones we obtained for the normal hearts. The graphs of parameter functions for the abnormal hearts, compare to those obtained for normal hearts, show less contraction towards the apex, less bending and more twisting in the abnormal hearts. From our experiments, we have been able to predict known differences. (Due to space limitation, we do not include the graphs and fitted models of all other hearts used in our experiments in this paper.)

Note that all fittings of models are within an acceptable error bound, since RMS errors are less than 5 %. Using only global parameter functions, our model provides the means of capturing and quantifying the LV motion and shape changes and quantitatively compare normal and abnormal hearts.

4 Conclusion

In this paper we presented a new class of physics-based deformable models which can deform both locally and globally. The characteristic of those models is that their global parameters are functions allowing the representation of complex shapes with a few intuitive parameters. For the applications in this paper we were able to eliminate many local parameters that require nontrivial processing to provide a compact representation of shape. We demonstrated the applicability of our technique to the shape character-

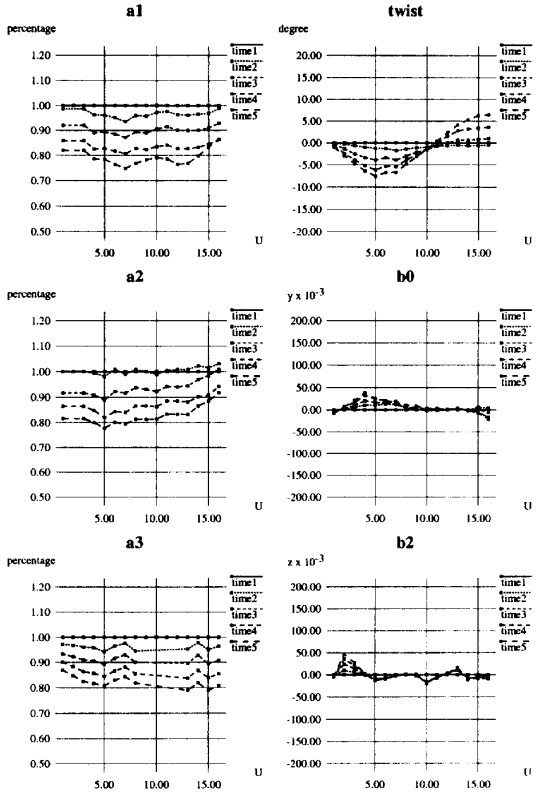

Figure 5: Extracted model parameters as functions of u.

ization of the LV for normal and abnormal hearts during systole, from MRI-SPAMM data. By plotting the parameter functions over time we were able to verify quantitatively qualitative knowledge about the LV motion common to physicians. We plan to apply our technique to multiple normal and abnormal hearts to be able to quantitatively characterize what is normal LV motion and what are the effects to the LV motion of the various LV diseases.

Acknowledgements

We would like to thank Dr. Ken Fellows, the director of the department of Radiology at the Children's Hospital of Philadelphia for his support for the project, and Dr. Leon Axel at the Hospital of University of Pennsylvania for providing us data sets to work with and for helpful discussions. The second author was supported by an NSF IRI-9309917 grant.

References

[1] A. Amini and J. Duncan. "Pointwise tracking of Left-Ventricular Motion in 3D," Proc. IEEE Workshop on Visual Motion, pp. 294-298, Princeton, NJ, 1991.

[2] L. Axel, L. Dougherty, "Heartwall motion: Improved method of spatial modulation of magnetization for MR imaging," *Radiology*, **172**, pp. 349-350, 1989.

[3] T. Binford. "Visual Perception by Computer", IEEE Conference on Systems and Control, Dec. 1971.

[4] L. D. Cohen and I. Cohen. "A Finite Element Method Applied to New Active Contour Models and 3D Reconstruction from Cross Sections", Proc. 2nd ICCV, pp. 587-591, Japan 1990.

[5] W-C. Huang and D. Goldgof. Adaptive-Size Meshes for Rigid and Nonrigid Shape Analysis and Synthesis. IEEE Transactions on Pattern Analysis, 15(6), pp. 611-616, 1993.

[6] M. Kass, A. Witkin and D. Terzopoulos. "Snakes: Active Contour Models", International Journal of Computer Vision, 1(4), pp. 321-331, 1988.

[7] D. Marr and K. Nishihara. "Representation and Recognition of the Spatial Organization of Three-Dimensional Shapes", Proc. Royal Society London B, 1978.

[8] T. McInerney and D. Terzopoulos. "A Finite Element Model for 3D Shape Reconstruction and Nonrigid Motion Tracking", Proc. 4th Int'l Conference on Computer Vision, pp. 518-523, Berlin, Germany, 1993.

[9] D.Metaxas, Physics-Based Modeling of Nonrigid Objects for Vision and Graphics, Ph.D. Thesis, Dept. of Computer Science, Univ. of Toronto, 1992.

[10] D. Metaxas and D. Terzopoulos. Shape and Nonrigid Motion Estimation Through Physics-Based Synthesis. *IEEE Trans. Pattern Analysis and Machine Intelligence*, 15(6), pp. 569-579 , June, 1993.

[11] C. Moore, W. O'Dell, E. McVeigh, E. Zerhouni, "Calculation of three-dimensional left ventricular strains form biplanar tagged MR images," *J Mag Res Imag* , **2**, pp. 165-175, 1992.

[12] A. Pentland and B. Horowitz. "Recovery of Nonrigid Motion and Structure". IEEE Pattern Analysis and Machine Intelligence, 13(7), pp. 730-742, July 1991.

[13] D.Terzopoulos and D. Metaxas. Dynamic 3D Models with Local and Global Deformations: Deformable Superquadrics. *IEEE Trans. Pattern Analysis and Machine Intelligence*, 13(7):703–714, 1991. See also Proc. Third International Conference on Computer Vision (ICCV'90), pp. 606-615, Osaka, Japan, Dec. 1990.

[14] A.A. Young, P.J. Hunter, B.H. Smaill, "Estimation of epicardial strain using the motions of coronary bifurcations in biplane cineangiography," *IEEE Trans Biomed Eng*, **39**, pp. 526-531, 1992.

[15] A.A. Young, L. Axel, "Three-dimensional Motion and Deformation of the Heart Wall"*Radiology*, **185**, pp. 241-247, 1992.